

An innovative unit operation of particle separation/classification by irradiating low-frequency ultrasound into water

メタデータ	言語: eng 出版者: 公開日: 2018-12-11 キーワード (Ja): キーワード (En): 作成者: Muramatsu, Hiroya, Saito, Takayuki メールアドレス: 所属:
URL	<a href="http://hdl.handle.net/10297/00026151">http://hdl.handle.net/10297/00026151</a>

**In print, AIChE Journal**

**An innovative unit operation of particle separation/classification by irradiating  
low-frequency ultrasound into water**

Hiroya Muramatsu<sup>1</sup> and Takayuki Saito<sup>2,\*</sup>

<sup>1</sup>Graduate School of Science and Technology, Shizuoka University, 3-5-1 Johoku, Naka-ku, Hamamatsu, Shizuoka 4328561, Japan.

<sup>2</sup>Research Institute of Green Science and Technology, Shizuoka University, 3-5-1 Johoku, Naka-ku, Hamamatsu, Shizuoka 4328561, Japan.

**\*Corresponding author:** Prof. Takayuki Saito, Research Institute of Green Science and Technology, Shizuoka University, 3-5-1 Johoku, Naka-ku, Hamamatsu, Shizuoka 4328561, Japan. Tel. & Fax: +81-53-478-1601. Email: [saito.takayuki@shizuoka.ac.jp](mailto:saito.takayuki@shizuoka.ac.jp)  
H. Muramatsu: [muramatsu.hiroya.15@shizuoka.ac.jp](mailto:muramatsu.hiroya.15@shizuoka.ac.jp)

## **Abstract**

By irradiating kHz-band ultrasound, submillimeter- or millimeter-size particles that were dispersed in water with dissolved gases flocculated into a spherically flocculated particle swarm (SFPS). Acoustic cavitation-oriented bubbles caused by the irradiation played essential roles in the formation of the SFPS. Unprecedented and promising phenomena were observed: the particles were separated based on their diameters through the precise control of the ultrasound irradiation, and the SFPS was easily manipulated by using a motion-controlled stick. We discuss the relationship between the sound-pressure profiles and the manipulable range of the SFPS; i.e., the effectively manipulable range was limited by the sound-pressure profile. By means of manipulation control, we demonstrate the particle classification by particle diameters. On the basis of these findings, we propose an example of a practical application of this technique.

## **Keywords**

kHz-ultrasound, separation, particle manipulation, acoustic cavitation-oriented bubbles, spherical particle flocculation

## Introduction

Separation/classification unit operations such as membrane separation, centrifugation separation, sedimentation and flotation are mandatory for high-performance, highly economic performance and low maintenance costs. Many researchers have been struggling with difficult issues of how to improve the efficiency and accuracy of the above technologies by focusing on the diameter, density and other aspects of the separation targets<sup>1-4</sup>. However, periodic maintenance is required to achieve the recovery from filter damage that is due to the friction between the membrane filter and the particles and to remove clogging of the membrane filter by the target particles<sup>5</sup>. Sieving techniques have been widely and industrially utilized for sizing particles, and have the advantages of a simple and low instrument cost apparatus. The sieving techniques, however, are not suited for the separation of emulsions or clayish agglomerated materials.

In light of the principles of centrifugation, the physical space of this method must be enlarged because high-speed rotation is necessary to accomplish the precise separation of particle diameters<sup>5</sup>. Ultrasound separation has the great advantages of non-invasive and a simple/small apparatus. Ultrasound technologies are used in oil/water separation of emulsion-type waste liquid<sup>6</sup>, fine particle manipulation<sup>7,8</sup>, ethanol enrichment from ethanol-water mixtures<sup>9</sup>, and size separation by ultrasound radiation in a microchannel<sup>10</sup>.

The demand for the removal of radioactive material (e.g., cesium) from wastewater has rapidly increased since the Fukushima Daiichi Nuclear Power Plant disaster in 2011<sup>11</sup>. A method of cesium adsorption on Prussian blue has been proposed<sup>12-17</sup>. Compared with some other adsorption materials such as zeolite, Prussian blue has a great advantage in that it provides affordable and highly efficient adsorption. Prussian blue nanoparticles are usually used as secondary particles (e.g., powder particles with the diameter of several tens of micrometers<sup>14</sup>, inorganic granules with diameters of several millimeters<sup>15</sup>, or nonwoven fabric<sup>15</sup>). Adsorption technology using column-packed Prussian blue beads is being considered for the purification of polluted radioactive wastewater. Parajuli et al. reported that the adsorption efficiency of cesium to Prussian blue particles varies with the secondary particle size<sup>17</sup>. In order to improve this technology which uses the secondary Prussian blue

particles, a new particle separation/classification technology that can be used to classify the Prussian blue particles by the particle diameter is urgently needed<sup>16, 17</sup>. We have been investigating ultrasound technologies to address this challenge.

Most of the conventional ultrasound separation technologies use MHz-band ultrasound because of its great advantages of high directionality and high acceleration. The principle of these separation technologies uses the acoustic radiation force acting directly on the separation target. Mitome summarized particle/bubble motions in sound-pressure fields<sup>18</sup>: a particle is trapped in the nodes/anti-nodes of the sound-pressure field, which depends on the density/compressibility of the particle/bubble. A bubble smaller than the resonant diameter is trapped at the anti-nodes, and a bubble larger than the resonant diameter is trapped at the nodes. However, in Mitome's study the target diameter was less than micrometer-order due to the limitation of the wavelength of the standing wave.

The past research using kHz-band ultrasound separation/manipulation technologies can be summarized as follows. Hatanaka<sup>19</sup> reported that polystyrene particles were trapped in a laminar-like pattern at the nodes of the sound-pressure field. Ohta<sup>20, 21</sup> proposed that the flocculation pattern of 16- $\mu\text{m}$ -diameter aluminum particles under 23- and 93-kHz ultrasound irradiation could be categorized into four types: band, point, clump and non-aggregation. Ochiai<sup>22</sup> proposed a three-dimensional particle manipulation system using computer-controlled 40-kHz ultrasound arrays in air. However, studies of particle separation and manipulation techniques using kHz-band ultrasound are very rare.

By irradiating 20-kHz ultrasound in water, we discovered an unprecedented and promising phenomenon in which dispersed particles with diameters from submillimeter- to millimeter-order are flocculated into a spherical swarm. Our previous study<sup>23</sup> revealed a part of this flocculation mechanism experimentally: a spherically flocculated particle swarm (SFPS) arose from the action of acoustic cavitation-oriented bubbles (ACOBs). We proposed a novel technology to separate and classify particles with diameters from a few hundred micrometers to a few millimeters by their diameter, by controlling the amplitude/frequency of the ultrasound radiation<sup>24</sup>.

We discovered another interesting phenomenon in which a motion-control stick near

the SFPS enables us to manipulate the SFPS. A practical operating system for both of the phenomena described above (i.e., the appearance of the SFPS and its manipulation with a motion-control stick) might be simple, and the combination of these phenomena might be very promising for completing urgent tasks such as the absorption of radioactive materials (e.g., radioactive cesium compounds) using Prussian blue particles. Here we propose an innovative particle separation/classification/manipulation technique using kHz-band ultrasound.

In this technique, we first measure the sound-pressure profiles (which decide the SFPS's behavior and controllability in the vessel) through a hydrophone. The motion of the SFPS and the reaction of the SFPS against the motion-control stick's motion are then analyzed on the basis of their visualized results. We discuss the relationship between the sound-pressure profiles and the motion of the SFPS, and we propose an environmentally friendly and new system that requires no chemical compound to separate and classify particles by their diameter, with the use of low-frequency ultrasound irradiation in water.

## **Experimental Setup**

### ***Experimental setup for the measurement of sound-pressure profiles***

Since the existence of ACOBs depends on temperature and atmospheric pressure and because the purpose of the present study was to collect fundamental and reliable data that would contribute to the design of a practical system, we conducted the experiments in a temperature-controlled room at  $22\pm 1^\circ\text{C}$ ,  $40\pm 3\%$  humidity and  $1000\pm 10$  hPa atmospheric pressure. The experimental setup for measuring the sound-pressure profile in an acrylic vessel was as described<sup>24</sup>. To measure the sound pressure three-dimensionally, we used motorized stages (SGSP46-300, Sigma Koki, Tokyo). A primary sine-wave signal from a function generator (SG-4105, Iwatsu, Tokyo) was amplified through an amplifier (2100L, E&I, Rochester, NY).

The amplified signal was inputted to a bolt-clamped Langevin-type transducer (HEC-45254M, Honda Electronics, Toyohashi, Japan) through a matching box; this transducer was tightly bonded to a stainless-steel plate attached to an acrylic vessel (inner

size: 54 mm × 54 mm, height: 200 mm, wall thickness: 3 mm). Sound-pressure profiles in the vessel were measured through a hydrophone (HPM1 and DC Coupler, Precision Acoustics, Dorset, UK). The motorized stages positioned the hydrophone's sensing tip (1-mm dia.) at any coordinates, and the hydrophone three-dimensionally scanned the inside of the vessel. The output signal of the hydrophone was stored in a digital recorder (8861-50, Hioki, Nagano, Japan). The size of the hydrophone's sensing tip was considered small enough to not influence the ultrasound field. Since the sampling rate of the output voltage from the hydrophone was set at 1 MHz, this rate was high enough to correctly measure the sound pressure of the examined 20-kHz-order ultrasound.

To avoid the adhesion of ACOBs on the hydrophone's sensing tip and to accurately acquire the sound-pressure profiles, we used only degassed water for this measurement. The degassed water was produced through a combined process (Fig. 1) of vacuum and ultrasound irradiation in ion-exchange water. One liter of ion-exchange water was put in a flask of capacity one liter, which was then set in the water bath. An outlet of the flask was connected to a vacuum pump (DAU-20, Ulvac, Chigasaki, Japan). The inside pressure of the flask was measured via a pressure gauge (KOT-401A, Daiichi Keiki, Tokyo) and controlled at  $-0.1$  MPaG during the degassing process.

Five BLT transducers (HEM-45254M, Honda Electronics) were attached to the bottom of the water bath. A primary sinuous signal of a function generator (SG-4105, Iwatsu) was amplified through an amplifier (2100L, E&I), and its impedance was adjusted by a matching box. The irradiation frequency and amplitude at the function generator were set at 24.8 kHz and 500 mV, respectively. The input power of the transducers was 54 W, which was greater than that during the measurement of the sound-pressure profiles. Thus, the ACOBs were not generated under the measurement of the sound-pressure profiles.

For the degassing of the dissolved gases, the transducers and vacuum pump were driven simultaneously for 10 min, and then a check valve (CVU8-8, Pisco, Nagano, Japan) was gradually opened to release the decompressed pressure to the atmosphere. The concentrations of CO<sub>2</sub> and O<sub>2</sub> were measured by a CO<sub>2</sub> meter (CGP-31, TOA, Kobe, Japan) and O<sub>2</sub> meter (HT2040-01, Hanna Instruments, Tokyo), respectively: 0.26 mM/L (CO<sub>2</sub>) and

0.03 mM/L (O<sub>2</sub>). The vessel was filled with this degassed water to a depth of 60–120 mm.

– Place Fig. 1 here –

### *Experimental setup for visualization of the SFPS*

The ion-exchange and dissolved gas concentration-controlled water described in the Section 2.1 above was used in this experiment. Figure 2 is the schematic for visualizing the motions of the motion-control stick and the SFPS. The driving system of the ultrasound is the same as that used for the sound-pressure measurement. Here the amplitude and frequency of the ultrasound irradiation were 500 mV and 20.0 kHz, respectively. The motion of a manipulating stick (5-mm dia.) made of PFA (AS ONE, Osaka, Japan) was controlled by the automatic stages (SGSP46-300, Sigma Koki) and their controller (SHOT-204MS, Sigma Koki).

Polystyrene particles (mean dia. 1000  $\mu\text{m}$ , density 1.06  $\text{g}/\text{cm}^3$ , average particle Reynolds number: 15.0, Sekisui Plastics, Osaka, Japan) were examined (see Fig. 3). The mass put in the vessel was set at 0.4 g (number of particles: 720). The stick motion and the SFPS motion were captured by a high-speed camera (FASTCAM SA-1.1, Photron, Yonezawa, Japan) with the following settings: image size, 1024  $\times$  1024 pixels; spatial resolution, 49.5  $\mu\text{m}/\text{pixel}$ ; frame rate, 250 fps; and exposure time, 1 ms. A flat LED (HF-SL-100WLCG, Raytronics, Saitama, Japan) was set on the opposite side of the high-speed camera and illuminated the objects. The stick's tip was set at  $(x, y, z) = (0, 0, 35)$ , and then the stick was traversed horizontally/vertically toward the wall/interface. The traverse speed of the stick was varied from 1 to 8 mm/s.

– Place Fig. 2 here –

– Place Fig. 3 here –

## **Results and Discussion**

## ***The sound-pressure profile***

### **The sound-pressure profile in the vessel**

Sound pressure profiles in the vessel should be discussed in terms of damped standing wave of the ultrasound. The damping of the ultrasound amplitude was caused mainly by ACOBs<sup>25</sup>. In the present study, we did not consider a simple standing wave because we conducted the sound-pressure measurement under the degassed water, and the ACOBs did not occur.

A typical result, i.e., normalized sound pressure on the center axis of the vessel, is plotted in Figure 4, where  $P_S(0, 0, z)$  is the measured sound pressure at  $x = 0, y = 0$  and  $z$ , and  $P_{S,Max}$  is the maximum value measured at  $x = 0, y = 0$  and  $z = 38.6$ .  $P_{S,Max}$  was the greatest sound-pressure value measured in the vessel. This curve of dimensionless sound pressure was numerically differentiated, and as a result, the following data were obtained: four extreme values (two local maximum values of  $P_{Lmax,1}$  and  $P_{Lmax,2}$  and two local minimum values of  $P_{Lmin,1}$  and  $P_{Lmin,2}$ ) and five inflection points ( $P_{Ipn}|_{n=1\sim 5}$ ).

The sound-pressure profile is composed of three convex-downward curves and three concave-upward curves. This profile is therefore different from a simple profile that is estimated to be a stationary wave given by  $\lambda=c/f$ , where  $\lambda$  represents the wavelength,  $c$  the sound speed and  $f$  the irradiated frequency.

The dimensionless sound-pressure profiles measured on planes of  $(4, 0, z)$ ,  $(8, 0, z)$ ,  $(12, 0, z)$ ,  $(16, 0, z)$  and  $(20, 0, z)$  are plotted in Figure 5a. As shown in the figure, although  $P_S(x, 0, z)/P_{S,Max}$  decreased with the increase in  $x$ , the shapes of the sound-pressure profiles except for those near the bottom are very similar to the profile measured at  $(0, 0, z)$ ; i.e., at  $z > 10$ , the shapes had two local maximum values, two local minimum values and four inflection points. The values of  $z$  taking the four extreme values into account are almost the same. In addition,  $P_S(x, 0, 70)/P_{S,Max}$ , e.g., at the water surface, are very similar. A counter of the normalized sound-pressure profile is illustrated in Figure 5b. The relationship between the manipulable range of the SFPS and the sound-pressure profile is discussed below.

– Place Fig. 4 here –

– Place Fig. 5 here –

### **Relationship between the sound-pressure profiles and the particle classification operation procedure**

We investigated the relationship between the sound-pressure profiles and the particle-classification operation. We first examined the effects of the water depth on the sound-pressure profiles. The normalized sound pressure (NSP) on the center axis of the vessel at 20-kHz ultrasound irradiation at the water depth of 60–120 mm is plotted in Figure 6. The wave traveling from the transducer was reflected at the water surface, and the traveling wave and the reflected wave were superimposed. As a result, a node of the sound pressure was formed at the water surface under these water-depth conditions. Under the water depth of 60 mm, the NSP reached the local maximum at  $z = 23.7$  mm (i.e., 36.3 mm from the water surface, this value is equal to one-half of the wavelength given by  $\lambda = c/f$ ).

Under the water depth of 120 mm, the NSP reached the local maximum values at  $z = 7.2$  (lower position) and at  $z = 84.0$  (upper position). The distance between the lower and upper positions is 76.8 mm, which is equal to the wavelength of the ultrasound. To trap particles at the multiple positions, the water depth must be set at a depth greater than one-and-a-half times the wavelength of the ultrasound, because the small-pressure-amplitude region (SPAR) is formed at the water surface. However, an excessively large water depth (e.g., 1 m) is not appropriate, because a sound-pressure field suitable for trapping the SPAR in the vessel is formed by the reflection of the sound wave due to the low directionality of the low-range ultrasound<sup>26</sup>. For instance, the water depth should be set at 120–150 mm under 20-kHz ultrasound irradiation into the water. The apparatus for this specific purpose should be composed of small and simple units; this compact size is a great advantage compared with the conventional sedimentation separation technique.

– Place Fig. 6 here –

We next investigated the effects of the amplitude of the output voltage of the function generator ( $V_{FG}$ ) on the sound-pressure profiles. The NSP on the vessel's center axis with 120-mm water depth is plotted in Figure 7a, with  $V_{FG}$  parameterizing. The amplitude of the sound pressure increased proportionally to  $V_{FG}$  (Fig. 7b). In contrast, the positions of the local maximum/minimum values were not shifted by changing  $V_{FG}$  (Fig. 7c). Here, it was difficult to simultaneously measure the sound pressure and the motions of both the stick and the SFPS because of the limitation of the size of the experimental setup; we therefore substituted the output voltage of the function generator for the sound-pressure amplitude.

– Place Fig. 7 here –

We assessed the effects of the irradiation frequency of the ultrasound on the NSP. The positions of the local maximum/minimum values shifted upward with the increase in the irradiation frequency. In addition, the sound-pressure amplitude near the transducer rose with the increase in the irradiation frequency. The input power into the vessel increased with the increase in the irradiation frequency, because the gap between the irradiation frequency and the resonant frequency of the apparatus was close. The changes of positions of the large-pressure-amplitude region (LPAR)/SPAR and the changes of the sound-pressure amplitude were caused by the change of the irradiation frequency.

### *Visualization of the SFPS manipulation*

#### *Horizontal manipulation*

Figure 8 shows typical results of the SFPS reaction to horizontal manipulations of the stick. Before the stick was manipulated horizontally ( $t < 2$  s), the SFPS was trapped at the LPAR next to the stick. With the insertion of a manipulation stick, the ACOBs were generated at the stick's surface. The ACOBs were attracted to each other because of secondary Bjerknes force under ultrasound irradiation. The ACOBs on the stick's surface attracted the SFPS. The SFPS followed the stick closely, at the same speed as the stick. By shifting the stick, the SFPS moved toward the SPAR, and the ACOB's surface motions were small. This indicates that the

secondary Bjerkens force became small. ACOBs at the LPAR (i.e., the center of the vessel) attracted the SFPS to the LPAR.

By shifting the stick further, the force acting on the SFPS from the LPAR became larger than that between the SFPS and the ACOBs near the stick. The SFPS was repelled from the stick at  $x = 5$ , and the repelling position of the SFPS did not depend on the manipulation speed. The effects of the manipulation speed were small because the ACOBs' surface motion synchronized with the irradiation frequency and the sound propagation speed was faster than the manipulation speed. The repelled SFPS returned to the center (i.e., the LPAR in the vessel) and went back and forth around the center of the vessel due to the SFPS's inertia. Interestingly, the SFPS maintained its diameter even though the SFPS was repelled from the stick. This indicates that our technique enables us to separate whole flocculated particles to a selected site (e.g., the position at which the particles were collected). This is a great advantage of this separation technique.

Figure 8b shows the results of the horizontal particle manipulation by varying  $V_{FG}$ . The stationary position in  $z$  decreased with the decrease in the sound-pressure amplitude. The stationary position of the SFPS before traversing the stick was the  $z$  of 44.0 at  $V_{FG} = 500$  mV, the  $z$  of 41.2 at  $V_{FG} = 400$  mV, and the  $z$  of 38.1 at  $V_{FG} = 300$  mV. The decline ratio of the stationary position was 3 mm per 100 mV. The amplitude of the sound pressure was proportional to the amplitude at the function generator. By decreasing the sound-pressure amplitude, the number of ACOBs generated in the vessel decreased; as a result, the motions of the ACOBs that induced the liquid motion in the vessel were weakened and small. We thus speculated that this change in the stationary position was the result of the change in the liquid motion induced by the motions of both the ACOBs and the particles, because the positions of the local maximum/minimum values were not changed by changing the amplitude of the function generator.

On the other hand, the SFPS's diameter and its motion in  $x$  direction against the stick motion did not depend on the output voltage of the function generator; the SFPS was released from the stick at  $x = 5.9$  mm, and was trapped at the LPAR with attenuation of the fluctuation. The SFPS's velocity moving with the stick at  $x = 0$  and the motion toward the LPAR were the

same. The average diameter of particle flocculation under these conditions was 9.5 mm. The number of flocculated particles was estimated as 550, and the flocculation ratio of the particles put in the vessel was 76%.

– Place Fig. 8 here –

### ***Vertical manipulation***

Figure 9 shows typical results of the vertical manipulation at  $v_s = 2, 4$  and  $8$  mm/s. The SFPS was trapped on the left side of the stick at  $z = 41.5$  before  $t < 2$  s. The SFPS moved toward the center of the vessel in  $x$  direction. The SFPS body moved with the stick until  $z = 47.4$  mm, and was then repelled from the stick. The flocculation body stayed at the center of the vessel again. The distance of the manipulation following the stick was approx. 6 mm, which was the same as the distance in the horizontal manipulation. As described above, the manipulable range of particles was closely related to the sound-pressure field.

– Place Fig. 9 here –

## **Our novel particle separation/manipulation technology proposal**

### ***Outline of the novel particle separation/manipulation technology***

We discovered that one can freely control and manipulate this type of particle flocculation by carefully adjusting the amplitude and frequency of the irradiated ultrasound. The snapshots in Figure 9 show the typical behavior of the interesting particle swarm. Dispersed particles with diameters from several hundred micrometers to several millimeters in water were flocculated into a spherical particle swarm by low-frequency ultrasound irradiation (Fig. 10a). The diameter of this initial SFPS was approx. 10 mm under 20-kHz band ultrasound irradiation. The SFPS was trapped in the LPAR in the vessel, due to acoustic radiation force acting on the ACOBs.

For example, by slightly decreasing the amplitude of the ultrasound, the flocculation position became lower, and the flocculated particle swarm could not maintain its spherical

shape; the collapse of the flocculation started on the outer edge of the particle swarm (Fig. 10b). With a further decrease in the amplitude, the collapse of the flocculation progressed (Fig. 10c).

In addition, as the amplitude decreased further, eventually all of the particles were dispersed widely, and they started settling down (Fig. 10d). At this point, the small particles settled more slowly than the large particles, because their settling velocities were lower than those of the large particles; the small particles were positioned on the upper side, and the large particles were positioned on the lower side. As the amplitude was dialed back to the initial value, the particles started to re-flocculate, and the small particles started to re-flocculate into a spherical swarm at the upper LPAR (Fig. 10e). The large particles started to re-flocculate at the lower LPAR (Fig. 10f). As the amplitude was set at the initial value, two stably spherical particle swarms were formed as shown in Fig. 10 g, h.

The diameter of the upper SFPS (Fig. 10 g) was 4.9 mm. The packing ratio of the upper SFPS was estimated at 56 - 60 %<sup>27</sup>. The number of the small particles flocculated in the upper SFPS was estimated at approx.1030, which indicated that the ratio of the flocculated particles in the upper SFPS to all the small particles put in the vessel was 10 %. The other small particles were dispersed in the vessel, or flocculated in the lower SFPS. All the particles composing the upper SFPS are manipulated by our manipulation technique. Thus, our separation technique provides at least 10 % of separation efficiency. This separation efficiency will be improved by the adjustment of ultrasound control (e.g., change rate of amplitude and frequency).

This separation technique can be applied not only for separation by the particle diameter but also by other particle properties (e.g., mass, density and wettability), because it is based on the sinking speed of the particles during the transition state of the amplitude/frequency modulation of the ultrasound. For instance, in examinations of density differences, small-density particles might be flocculated at the upper LPAR, and large-density particles might be flocculated at the lower LPAR. It is also possible that our system can be used for separation on the basis of the wettability of the particles. Hydrophobic particles might be trapped more easily than hydrophilic particles, because particles need ACOBs

adhering to their surface in order to flocculate.

– **Place Fig. 10 here** –

Figure 11 shows that the SFPS is easily manipulated in a simple manner. Just after the manipulation stick was inserted near the initial SFPS, the SFPS gradually moved toward the manipulation stick. The SFPS moved with the motion of the manipulation stick.

– **Place Fig. 11 here** –

### ***Application of this separation system in an industrial or environmental field***

As stated above, our technology is effective for separating particles with the same density and different diameters. When our technology is applied to the treatment of wastewater that includes radioactive cesium by means of the adsorption of cesium into Prussian blue particles, the particles after cesium adsorption must be accurately and effectively separated in accord with the particles' size and density in order to decrease the environmental and economic post-treatment loads. We consider a two-step separation process: the first step of separation by size and a second step of separation by density, on the basis of the finding that the adsorption efficiency of cesium into the Prussian blue particles was affected by their diameter<sup>17</sup>.

In the size separation (the first-step separation), Prussian blue particles with target diameters effective for the second-step separation are used. In the density separation (the second-step separation), Prussian blue particles with the target density (i.e. the target adsorption amount of cesium) are separated. The Prussian blue particles having fully adsorbed the radioactive cesium can be disposed of in post-processing. The remaining Prussian blue particles which have imperfectly adsorbed the radioactive cesium could be reused. Thus, using this two-step separation process, a volume reduction of radioactive waste will be achieved.

The manipulable range of particle swarms in the present experiments was 6 mm, and

this range was the result of the sound-pressure distribution. By shifting the sound-pressure profile with the particle manipulation using a multi-transducer array system like that described by Ochiai<sup>22</sup>, the SFPS can be manipulated over a long distance. To apply our technique to a practical process, we need to conduct further research to evaluate the recovery efficiency of polluted Prussian blue beads. We also need to clarify aspects of the mechanisms underlying the flocculation and manipulation, such as the interactions among the particles, the ACOBs and the surrounding liquid motion.

## **Conclusions**

Millimeter-size particles dispersed in dissolved-gases water are flocculated into a spherical swarm (the SFPS) by irradiation with kHz-band ultrasound. We revealed the flocculation mechanism in which ACOBs play a role in forming the SFPS. The SFPS can be manipulated easily by a motion-controlled stick. We propose a novel particle separation/classification and manipulation technique. In the present study, we investigated the relationship between the sound-pressure profile and the motions of the stick and SFSP. First, we measured the sound-pressure profiles in the vessel via a scanning hydrophone. The motions of the SFPS and the stick were then analyzed. The SFPS maintained its formation as it followed the stick. The horizontal/vertical manipulable range of the SFPS was approx. 6 mm. After the stick was released from the SFPS, the SFPS was trapped at the large-pressure-amplitude region with attenuation of the flocculation. The SFPS's manipulable range and its motion were closely related to the sound-pressure profiles in the vessel. On the basis of these results, we demonstrated particle size classification by precise control of the ultrasound irradiation. Combining particle classification and manipulation processes, we have proposed industrial applications using kHz-band ultrasound for separation processes. Our present results also demonstrated that our technique has a high potential for use in separation applications for not only particle diameters but also other particle properties.

## **Acknowledgements**

This study was promoted and financially supported by Category "A" of the Grants-in-Aid for

Scientific Research, the Japan Society for the Promotion of Science (JSPS). We thank the JSPS for its help. We declare no conflicts of interest.

## Literature Cited

1. Ciardelli G, Corsi L, Marcucci M. Membrane separation for wastewater reuse in the textile industry. *Resour Conserv Recycl.* 2000;31:189-197.  
doi:10.1016/S0921-3449(00)00079-3.
2. Akbulut O, MacE CR, Martinez R V., et al. Separation of nanoparticles in aqueous multiphase systems through centrifugation. *Nano Lett.* 2012;12(8):4060-4064.  
doi:10.1021/nl301452x.
3. Ha Z, Liu S. Settling velocities of polydisperse concentrated suspensions. *Can J Chem Eng.* 2002;80(October):783-790.  
<http://onlinelibrary.wiley.com/doi/10.1002/cjce.5450800501/abstract>.
4. Rubio J, Souza ML, Smith RW. Overview of flotation as a wastewater treatment technique. *Miner Eng.* 2002;15(3):139-155. doi:10.1016/S0892-6875(01)00216-3.
5. Cain CW, Zievers JF, Emmett RC, Ambler CM, Nickolaue N, Wrotnowski AC, Kominek EG, Lash LD, Day RW, Grichar CN. Solid-Liquid Mixtures. In: Schweitzer PA. *Handbook of Separation Techniques for Chemical Engineers.* New York: McGraw-Hill, 1979:4-3– 4-140.
6. Nii S, Kikumoto S, Tokuyama H. Quantitative approach to ultrasonic emulsion separation. *Ultrason Sonochem.* 2009;16(1):145-149.  
doi:10.1016/j.ultsonch.2008.07.005.
7. Kozuka T, Tuziuti T, Mitome H, Fukuda T. Control of a standing wave field using a line-focused transducer for two-dimensional manipulation of particles. *Japanese J Appl Physics, Part 1 Regul Pap Short Notes Rev Pap.* 1998;37(5 SUPPL. B):2974-2978.  
doi:10.1143/JJAP.37.2974.
8. Sobanski MA, Robert Tucker C, Thomas NE, Terence Coakley W. Sub-micron particle manipulation in an ultrasonic standing wave: Applications in detection of clinically important biomolecules. *Bioseparation.* 2000;9(6):351-357.  
doi:10.1023/A:1011175404581.
9. Kirpalani DM, Suzuki K. Ethanol enrichment from ethanol-water mixtures using high

- frequency ultrasonic atomization. *Ultrason Sonochem.* 2011;18(5):1012-1017.  
doi:10.1016/j.ultsonch.2010.05.013.
10. Kapishnikov S, Kantsler V, Steinberg V. Continuous particle size separation and size sorting using ultrasound in a microchannel. *J Stat Mech Theory Exp.* 2006;2006(1):P01012-P01012. doi:10.1088/1742-5468/2006/01/P01012.
  11. Yasunari TJ, Stohl A, Hayano RS, Burkhart JF, Eckhardt S, Yasunari T. Cesium-137 deposition and contamination of Japanese soils due to Fukushima nuclear accident. *PNAS.* 2011;108(49):19530–19534. doi: 10.1073/pnas.1112058108.
  12. Thammawong C, Opaprakasit P, Tangboriboonrat P, Sreearunothai P. Prussian blue-coated magnetic nanoparticles for removal of cesium from contaminated environment. *J Nanoparticle Res.* 2013;15(6). doi:10.1007/s11051-013-1689-z.
  13. Hu B, Fugetsu B, Yu H, Abe Y. Prussian blue caged in spongiform adsorbents using diatomite and carbon nanotubes for elimination of cesium. *J Hazard Mater.* 2012;217-218:85-91. doi:10.1016/j.jhazmat.2012.02.071.
  14. Fujita H, Sasano H, Miyajima R, Sakoda A. Adsorption equilibrium and kinetics of cesium onto insoluble Prussian blue synthesized by an immediate precipitation reaction between  $\text{Fe}^{3+}$  and  $[\text{Fe}(\text{CN})_6]^{4-}$ . *Adsorption.* 2014;20(7):905-915. doi:10.1007/s10450-014-9635-7.
  15. Chen GR, Chang YR, Liu X, Kawamoto T, Tanaka H, Kitajima A, Parajuli D, Takasaki M, Yoshino K, Chen ML, Lo YK, Lei Z, Lee DJ. Prussian blue (PB) granules for cesium (Cs) removal from drinking water. *Sep Purif Technol.* 2015;143:146-151. doi:10.1016/j.seppur.2015.01.040.
  16. Bang H, Watanabe K, Nakashima R, et al. A highly hydrophilic water-insoluble nanofiber composite as an efficient and easily-handleable adsorbent for the rapid adsorption of cesium from radioactive wastewater. *RSC Adv.* 2014;4(103):59571-59578. doi:10.1039/C4RA09713K.
  17. Parajuli D, Kitajima A, Takahashi A, et al. Application of Prussian blue nanoparticles for the radioactive Cs decontamination in Fukushima region. *J Environ Radioact.* 2016;151:233-237. doi:10.1016/j.jenvrad.2015.10.014.

18. Mitome H. Micro bubble and sonoluminescence. *Japanese J Appl Physics, Part 1 Regul Pap Short Notes Rev Pap*. 2001;40(5 B):3484-3487. doi:10.1143/JJAP.40.3484.
19. Hatanaka SI, Taki T, Kuwabara M, Sano M, Asai S. Effect of process parameters on ultrasonic separation of dispersed particles in liquid. *Japanese J Appl Physics, Part 1 Regul Pap Short Notes Rev Pap*. 1999;38(5 B):3096-3100. doi:10.1143/JJAP.38.3096.
20. Ohta J, Makara T, Hirobe S. Effects of Ultrasound on Behavior of Fine Solid Particles in Solid-liquid Mixture (1st Report, Horizontal Irradiation in Stationary Solid-liquid Mixture). *Trans Japan Soc Mech Eng Ser B*. 2005;71(701):125-132. doi:10.1299/kikaib.71.125.
21. Ohta J, Nakano H. Effects of Ultrasound on Behavior of Fine Solid Particles in Solid-Liquid Mixture (Classification of Particle Aggregation and Sound Pressure Profiles under Horizontal Irradiation). *J Fluid Sci Technol*. 2008;3(5):655-666. doi:10.1299/jfst.3.655.
22. Ochiai Y, Hoshi T, Rekimoto J. Three-dimensional mid-air acoustic manipulation by ultrasonic phased arrays. *PLoS One*. 2014;9(5):1-5. doi:10.1371/journal.pone.0097590.
23. Mizushima Y, Nagami Y, Nakamura Y, Saito T. Interaction between acoustic cavitation bubbles and dispersed particles in a kHz-order-ultrasound-irradiated water. *Chem Eng Sci*. 2013;93:395-400. doi:10.1016/j.ces.2013.02.028.
24. Muramatsu H, Yanai S, Mizushima Y, Saito T. A novel particle separation technique using 20-kHz-order ultrasound irradiation in water. *J Phys Conf Ser*. 2015;656:12117. doi:10.1088/1742-6596/656/1/012117.
25. Yasui K. Fundamentals of Acoustic Cavitation and Sonochemistry. Pankaj, Ashokkumar M. In: *Theoretical and Experimental Sonochemistry Involving Inorganic Systems*. New York: Springer, 2011:20-25.
26. Asakura Y, Nishida T, Matsuoka T, Koda S. Effects of ultrasonic frequency and liquid height on sonochemical efficiency of large-scale sonochemical reactors. *Ultrason Sonochem*. 2008;15(3):244-250. doi:10.1016/j.ultsonch.2007.03.012.
27. Muramatsu H, Saito T. The relationship between bubble motion and particle flocculation pattern under 20-kHz-ultrasound radiation in water. *Chem Eng Sci*. 2017;170:195-203.

doi:10.1016/j.ces.2017.03.040.

## Figure Captions

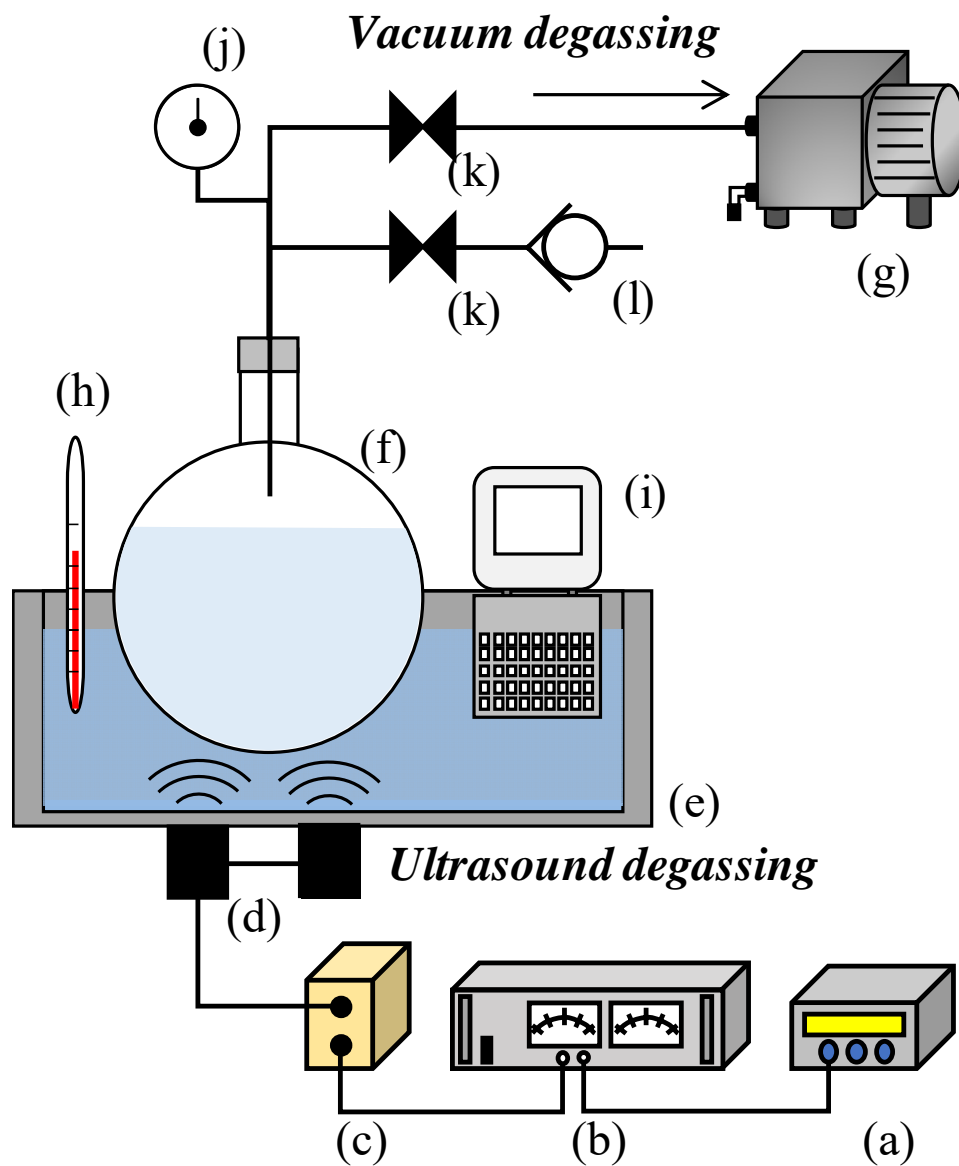


**Fig. 1.** Schematic of the degassing setup. **a:** Function generator, **b:** Amplifier, **c:** Matching box, **d:** Transducer, **e:** Water tank, **f:** Flask, **g:** Vacuum pump, **h:** Thermometer, **i:** Thermostat, **j:** Pressure gage, **k:** Valve, **l:** Check valve.

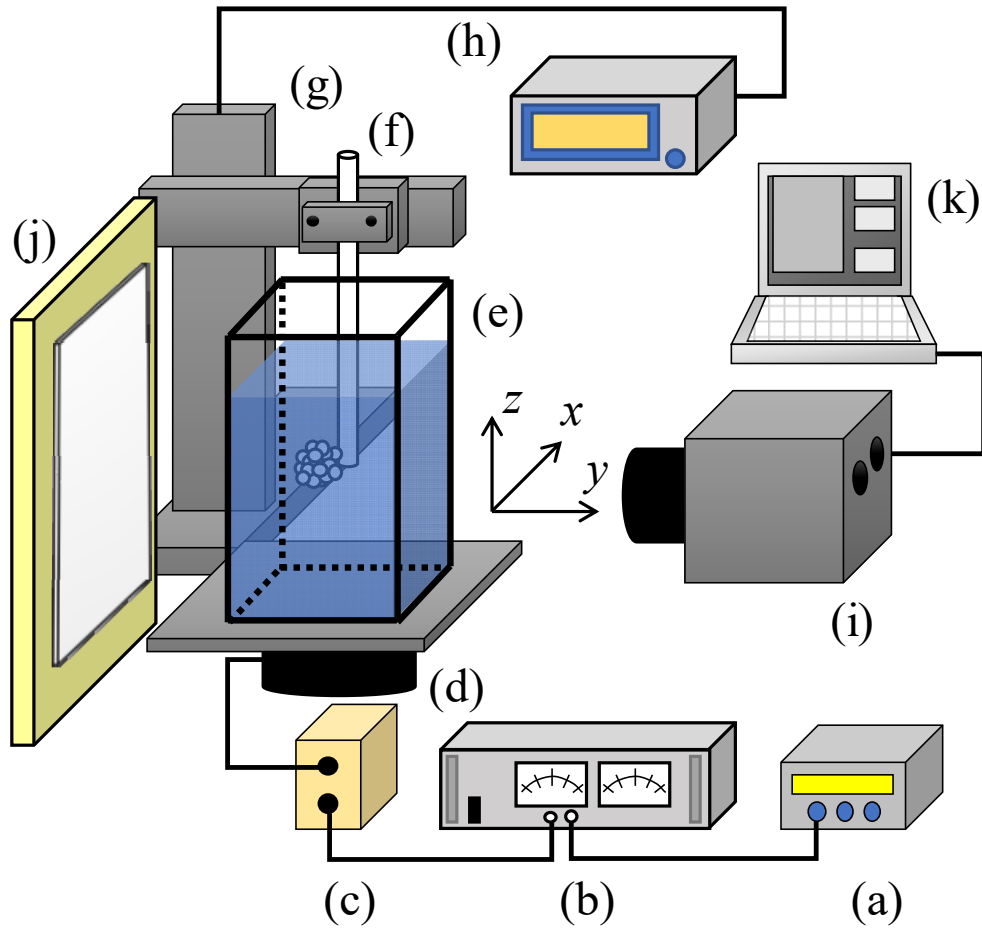


**Fig. 2.** The experimental setup for capturing the ACOBs' distribution near the motion-control stick. **a:** Function generator, **b:** Amplifier, **c:** Matching box, **d:** Transducer, **e:** Acrylic vessel, **f:** Stick, **g:** Motorized stage, **h:** Stage controller, **i:** High-speed video camera, **j:** LED light, **k:** PC.

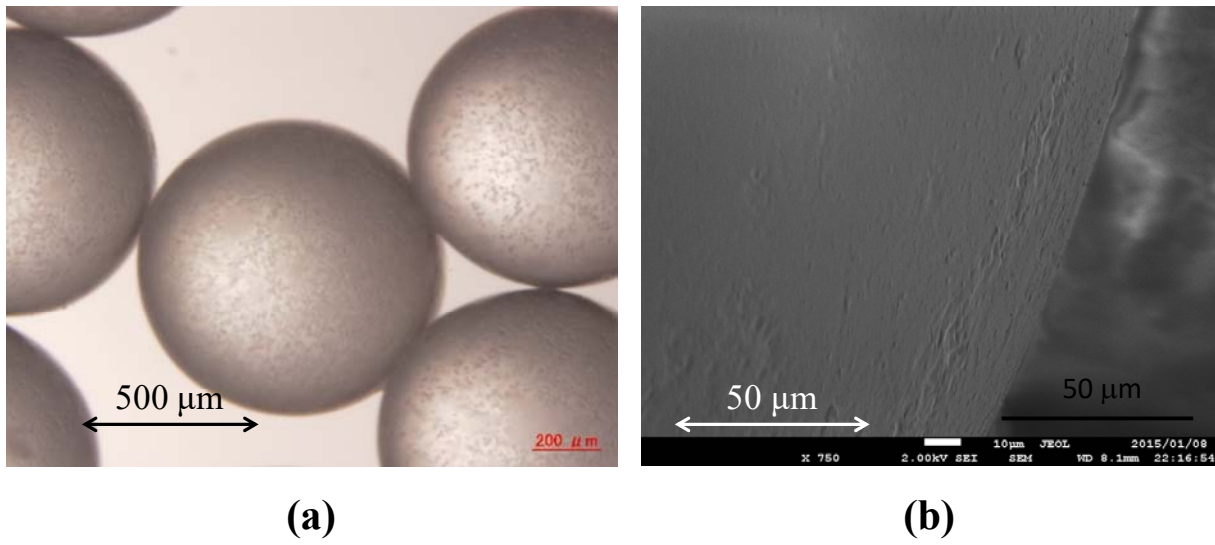


**Fig. 3.** Typical images of the polystyrene particles in the present study. **a:** Microscopic image, **b:** SEM image of the particle surface.

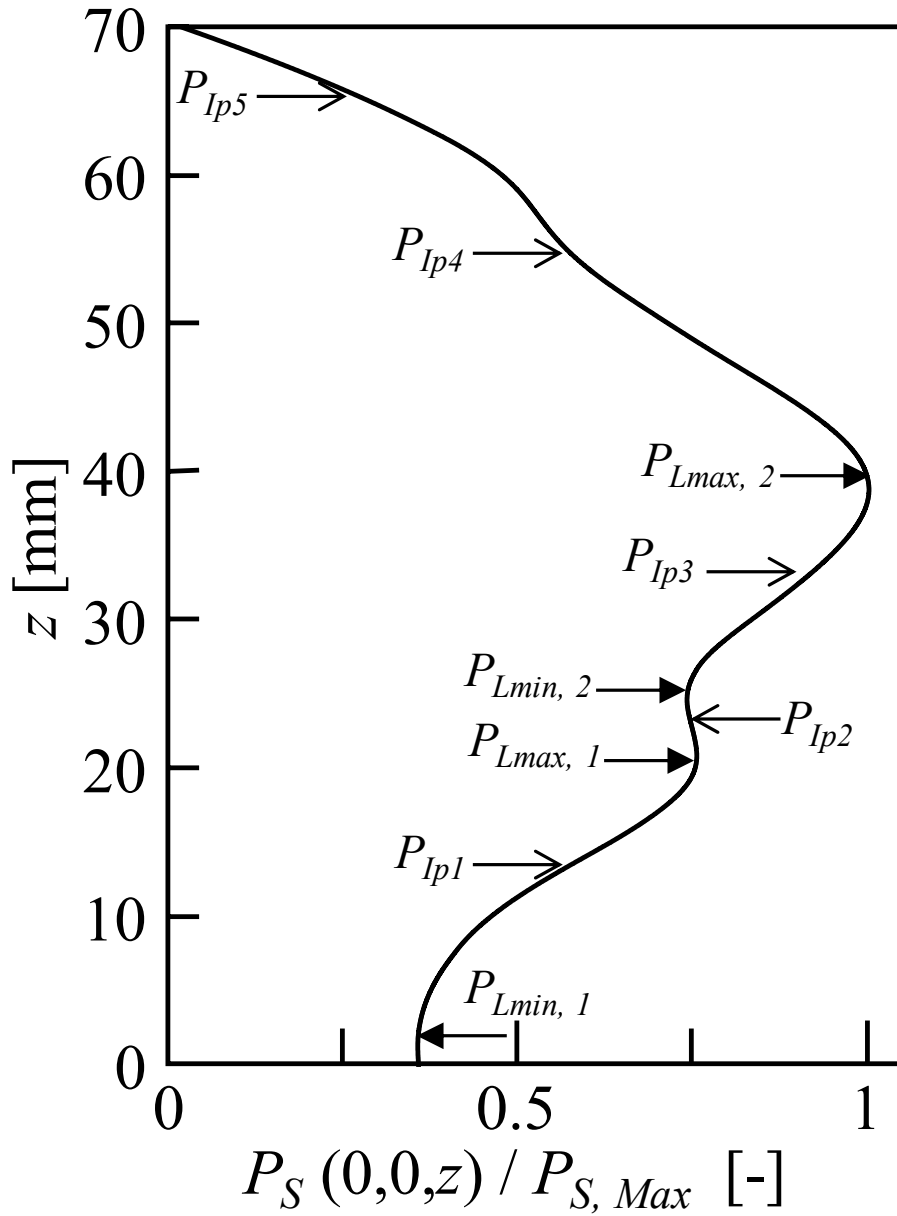


**Fig. 4.** A typical sound-pressure profile on the center axis  $(0, 0, z)$  of the vessel. Plots of sound pressure normalized by the maximum sound pressure  $P_{S, Max}$  measured at  $(0, 0, 38.6)$ . " $z = 0$ " indicates the bottom of the vessel, and " $z = 70$ " indicates the water surface.

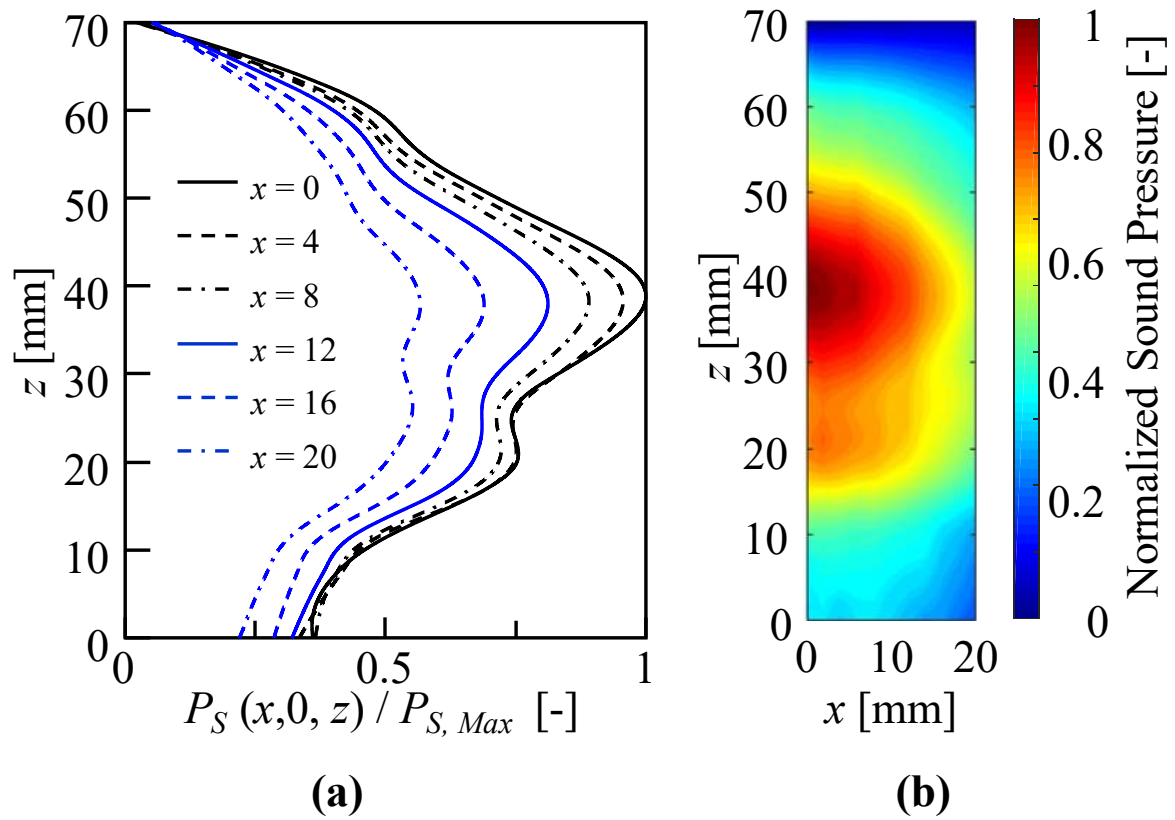


**Fig. 5.** Sound-pressure profiles on the center plain ( $x, 0, z$ ) of the vessel. **a:** Sound pressure profiles normalized by the maximum sound pressure at  $(0, 0, 38.6)$ . **b:** Contour map of the normalized sound-pressure field at the center plane in the right side of the vessel.

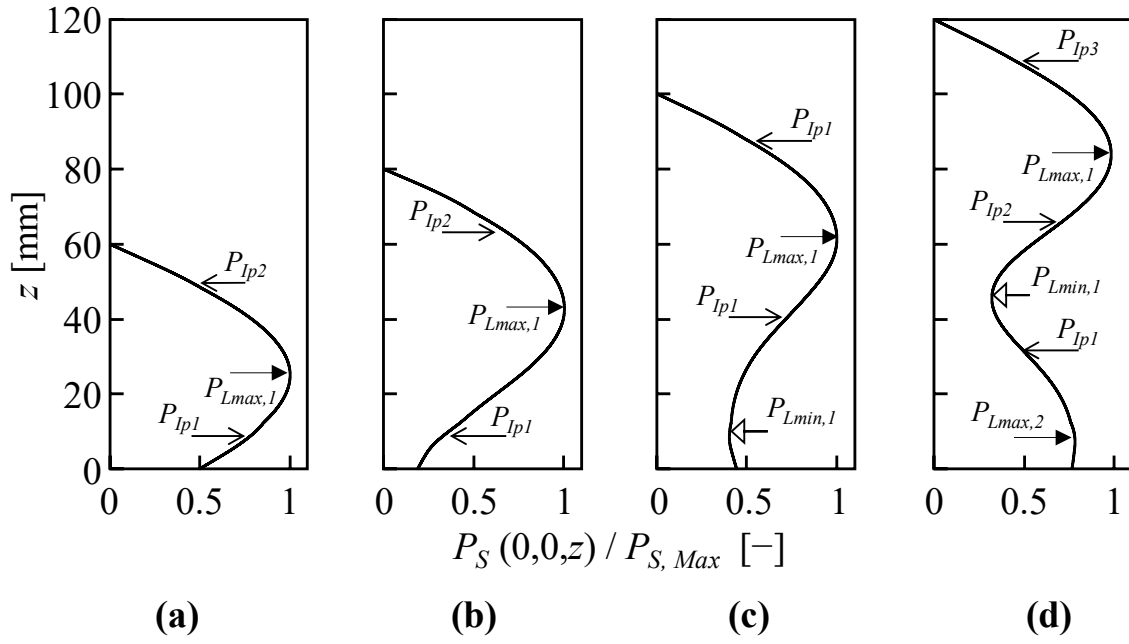


**Fig. 6.** Normalized sound-pressure profiles on the center axis (0, 0, z) of the vessel under 20-kHz ultrasound irradiation, with varying water depths: **a:** 60 mm, **b:** 80 mm, **c:** 100 mm, **d:** 120 mm.

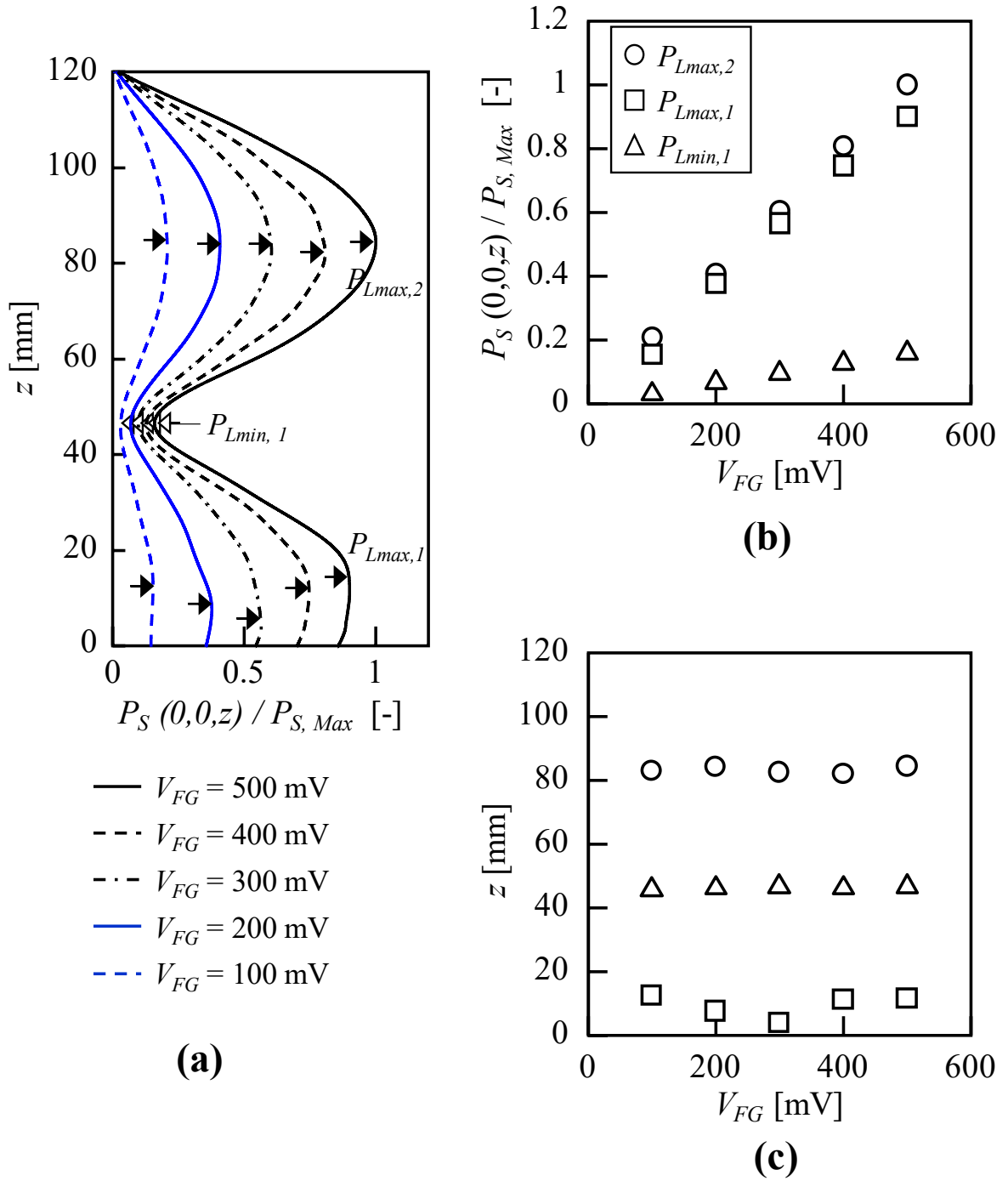


**Fig. 7.** Effect of input power on the normalized sound-pressure profiles at the water depth of 120 mm. **a:** Sound pressure profiles normalized by the maximum sound pressure at (0, 0, 84.0). **b:** The relationship between the input power and the amplitude of the sound pressure. **c:** The relationship between the input power and the position of the local maximum/minimum value.

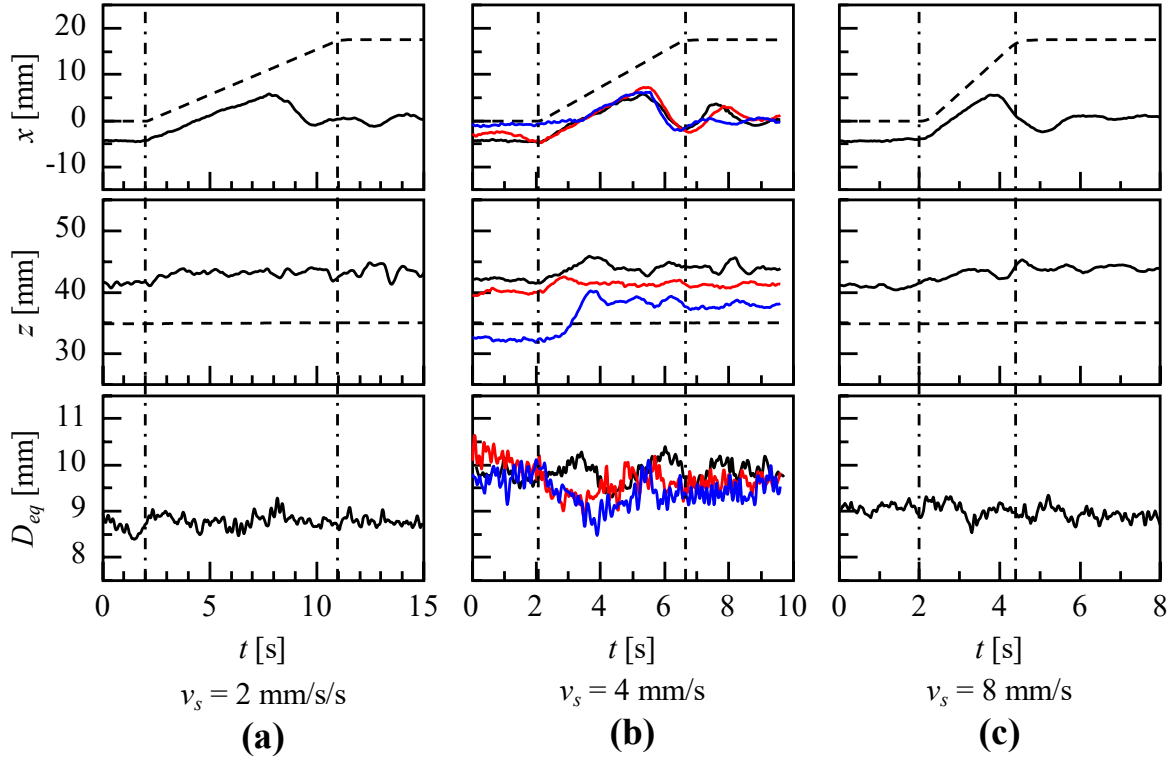


**Fig. 8.** Typical results of motions of both the motion-control stick and the SFPS by varying the stick speed ( $v_s$ ) from 1 to 8 mm/s: **(a)** 2 mm/s; **(b)** 4 mm/s; **(c)** 8 mm/s. Solid lines: the SFPS's motion. Broken lines: the stick's motion. Black chain lines: the time of the start and stopping of the horizontal-stick manipulation. Colors in (b) indicate the results of the SFPS's motion under the variation of the input power. Black line:  $V_{FG} = 500$  mV. Red line:  $V_{FG} = 400$  mV. Blue line:  $V_{FG} = 300$  mV.

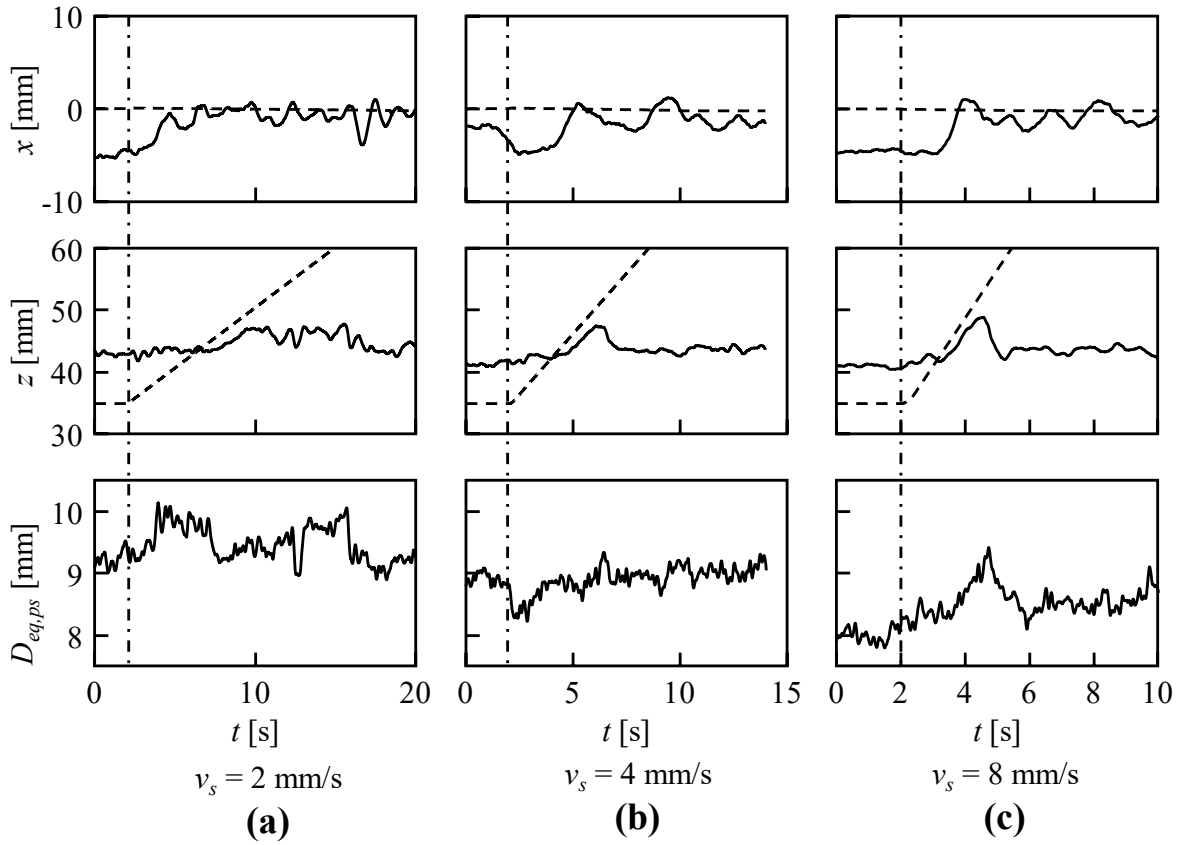


**Fig. 9.** Typical results of motions of both the stick and the SFPS by varying the stick speed ( $v_s$ ) from 1 to 8 mm/s: **(a)** 2 mm/s; **(b)** 4 mm/s; **(c)** 8 mm/s. Solid lines: the SFPS's motion. Broken lines: the stick's motion. Black chain lines: the time of the start of the vertical stick movement.

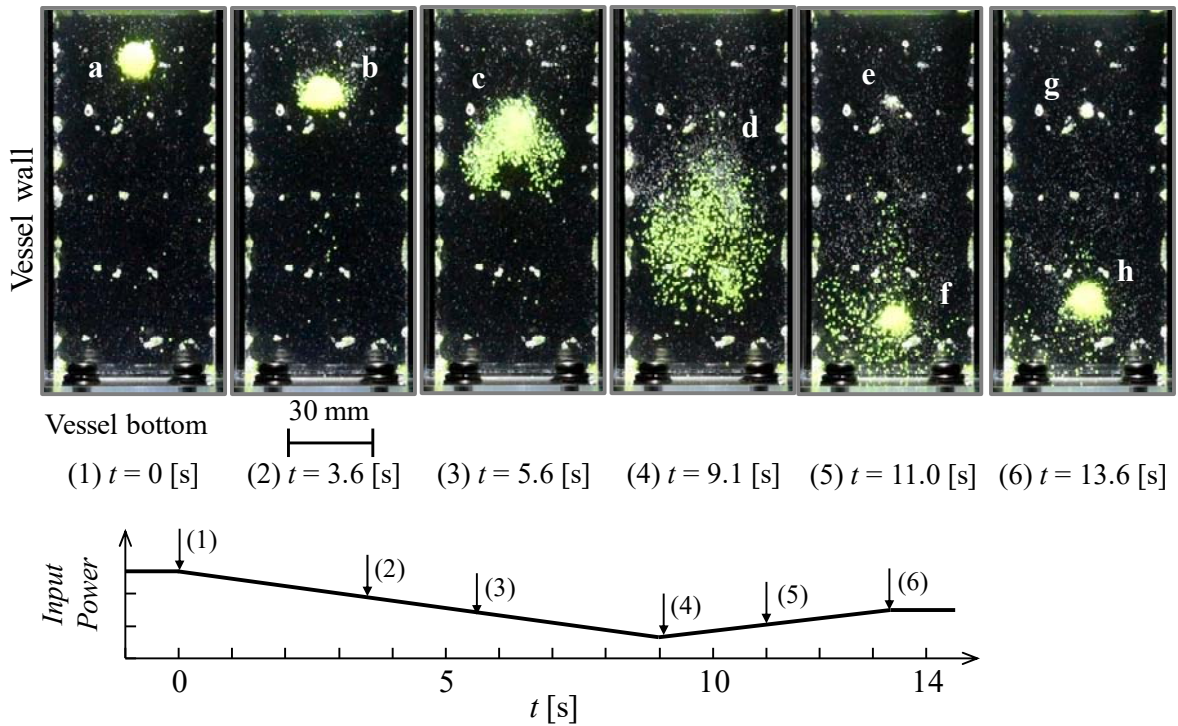


**Fig. 10.** Snapshots of the particle classification by their diameters, by adjusting the input power of the ultrasound irradiation (upper) and the amplitude change of the input power (bottom). White particles: diameter 400  $\mu\text{m}$ , density 1.06  $\text{g}/\text{cm}^3$ . Yellow particles: diameter 800  $\mu\text{m}$ , density 1.06  $\text{g}/\text{cm}^3$ . (1) The start time of the amplitude change. **a:** The initial SFPS composed of the mixed particles. (2) and (3) The transition state of the decrease in the input power. **b:** The deterioration and settling of the SFPS composed of the mixed particles. **c:** More deterioration and the falling of the SFPS composed of the mixed particles. (4) The time period during the change of the input power from decreasing to increasing. **d:** No particle flocculation (completely dispersed particles). (5) The transition state of the increment of the input power. **e:** Growth of a new SFPS composed of the smaller-dia. particles. **f:** Growth of the larger-dia. particles. (6) The finish time of the particle separation. **g:** The fully developed SFPS composed of the smaller-dia. particles. **h:** The fully developed SFPS composed of the larger-dia. particles.

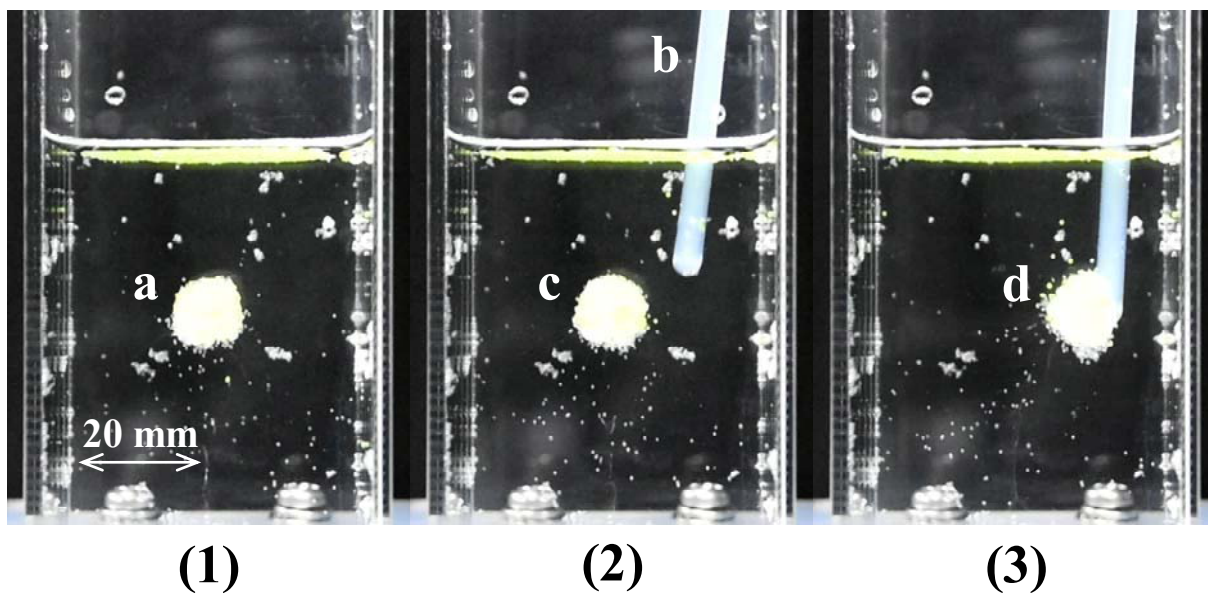


**Fig. 11.** Snapshots of the SFPS manipulation. **a:** Initial SFPS of 1-mm-dia. particles. **b:** Control stick inserted in the water. **c:** The SFPS gradually moving toward the stick. **d:** The SFPS moving with the stick and trapped at the side and edge of the stick.